

Title	A comparative study of the structural, mechanical and tribological characteristics of TiSiC-Cr coatings prepared in CH <sub>4</sub> and C <sub>2</sub> H <sub>2</sub> reactive atmosphere by cathodic vacuum arc
Authors	Braic, Mariana;Vladescu, Alina;Balaceanu, Mihai;Luculescu, Catalin;Padmanabhan, Siby C.;Constantin, Lidia;Morris, Michael A.;Braic, V.;Grigorescu, Cristiana E. A.;Ionescu, Paul;Dracea, Maria Diana;Logofatu, Constantin
Publication date	2017-12-21
Original Citation	Braic, M., Vladescu, A., Balaceanu, M., Luculescu, C., Padmanabhan, S. C., Constantin, L., Morris, M. A., Braic, V., Ana Grigorescu, C. E., Ionescu, P., Dracea, M. D. and Logofatu, C. (2017) 'A comparative study of the structural, mechanical and tribological characteristics of TiSiC-Cr coatings prepared in CH <sub>4</sub> and C <sub>2</sub> H <sub>2</sub> reactive atmosphere by cathodic vacuum arc', Applied Surface Science, 400, pp. 318-328. doi:10.1016/j.apsusc.2016.12.160
Type of publication	Article (peer-reviewed)
Link to publisher's version	10.1016/j.apsusc.2016.12.160
Rights	© 2016 Elsevier B.V. All rights reserved. This manuscript version is made available under the CC-BY-NC-ND 4.0 license <a href="http://creativecommons.org/licenses/by-nc-nd/4.0/">http://creativecommons.org/licenses/by-nc-nd/4.0/</a> - <a href="http://creativecommons.org/licenses/by-nc-nd/4.0/">http://creativecommons.org/licenses/by-nc-nd/4.0/</a>
Download date	2025-03-23 10:14:23
Item downloaded from	<a href="https://hdl.handle.net/10468/3460">https://hdl.handle.net/10468/3460</a>



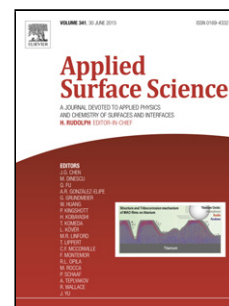
# UCC

**University College Cork, Ireland**  
Coláiste na hOllscoile Corcaigh

## Accepted Manuscript

Title: A comparative study of the structural, mechanical and tribological characteristics of TiSiC-Cr coatings prepared in CH<sub>4</sub> and C<sub>2</sub>H<sub>2</sub> reactive atmosphere by cathodic vacuum arc

Author: Mariana Braic Alina Vladescu Mihai Balaceanu  
Catalin Luculescu Sibiu C. Padmanabhan Lidia Constantin  
Michael A. Morris Viorel Braic Cristiana Eugenia Ana  
Grigorescu Paul Ionescu Maria Diana Dracea Constantin  
Logofatu



PII: S0169-4332(16)32892-6  
DOI: <http://dx.doi.org/doi:10.1016/j.apsusc.2016.12.160>  
Reference: APSUSC 34707

To appear in: *APSUSC*

Received date: 14-7-2016  
Revised date: 16-12-2016  
Accepted date: 19-12-2016

Please cite this article as: Mariana Braic, Alina Vladescu, Mihai Balaceanu, Catalin Luculescu, Sibiu C. Padmanabhan, Lidia Constantin, Michael A. Morris, Viorel Braic, Cristiana Eugenia Ana Grigorescu, Paul Ionescu, Maria Diana Dracea, Constantin Logofatu, A comparative study of the structural, mechanical and tribological characteristics of TiSiC-Cr coatings prepared in CH<sub>4</sub> and C<sub>2</sub>H<sub>2</sub> reactive atmosphere by cathodic vacuum arc, Applied Surface Science <http://dx.doi.org/10.1016/j.apsusc.2016.12.160>

This is a PDF file of an unedited manuscript that has been accepted for publication. As a service to our customers we are providing this early version of the manuscript. The manuscript will undergo copyediting, typesetting, and review of the resulting proof before it is published in its final form. Please note that during the production process errors may be discovered which could affect the content, and all legal disclaimers that apply to the journal pertain.

**Highlights**

- TiSiC-Cr coatings were deposited via cathodic arc evaporation.
- The coatings derived from C<sub>2</sub>H<sub>2</sub> outperformed those prepared in CH<sub>4</sub> plasma.
- The coatings consisted of a mixture of crystalline solid solution carbide and amorphous hydrogenated carbon phases.
- The coatings produced with C<sub>2</sub>H<sub>2</sub> exhibited the highest hardness, the lowest friction coefficient and wear resistance.

**A comparative study of the structural, mechanical and tribological characteristics  
of TiSiC-Cr coatings prepared in CH<sub>4</sub> and C<sub>2</sub>H<sub>2</sub> reactive atmosphere  
by cathodic vacuum arc**

Mariana Braic<sup>1</sup>, Alina Vladescu<sup>1\*</sup>, Mihai Balaceanu<sup>1</sup>, Catalin Luculescu<sup>2</sup>, Sibiu C.  
Padmanabhan<sup>3,4\*</sup>, Lidia Constantin<sup>1</sup>, Michael A. Morris<sup>3,4</sup>, Viorel Braic<sup>1</sup>, Cristiana Eugenia  
Ana Grigorescu<sup>1</sup>, Paul Ionescu<sup>5</sup>, Maria Diana Dracea<sup>5</sup>, Constantin Logofatu<sup>6</sup>

<sup>1</sup>National Institute for Optoelectronics, 409 Atomistilor St., Magurele-Bucharest, Romania

<sup>2</sup>National Institute for Laser, Plasma and Radiation Physics, 409 Atomistilor St.,  
077125 Magurele-Bucharest, Romania

<sup>3</sup>University College Cork, Department of Chemistry, College Road, Cork, Ireland

<sup>4</sup>Advanced Materials and BioEngineering Research (AMBER), Trinity College Dublin,  
College Green, Dublin 2, Ireland

<sup>5</sup>Horia Hulubei National Institute in Physics and Nuclear Engineering, 30 Reactorului St.,  
077125 Magurele-Bucharest, Romania

<sup>6</sup>National Institute of Materials Physics, 105bis Atomistilor  
St., 077125 Magurele-Bucharest, Romania

Abstract

TiSiC-Cr coatings, with Cr and Si as additional elements, were deposited on Si, C 45 and 316 L steel substrates via cathodic arc evaporation. Two series of coatings with thicknesses of 3.6–3.9 μm were produced, using either CH<sub>4</sub> or C<sub>2</sub>H<sub>2</sub> as carbon containing gas. For each series, different coatings were prepared by varying the carbon rich gas flow rate between 90 and 130 sccm, while maintaining constant cathode currents (110 and 100 A at TiSi and Cr cathodes, respectively), substrate bias (-200 V) and substrate temperature (~320 °C). The coatings were analyzed for their mechanical characteristics (hardness, adhesion) and

---

\* Corresponding authors: Alina Vladescu (Tel./Fax: +4-021-457.57.59, email: alinava@inoe.ro ) and Sibiu C. Padmanabhan (Tel./Fax: +353-21-427-4097, email: sc.padmanabhan@ucc.ie ).

tribological performance (friction, wear), along with their elemental and phase composition, chemical bonds, crystalline structure and cross-sectional morphology.

The coatings were found to have nano-scale composite structures consisting of carbide crystallites (grain size of 3.1–8.2 nm) and amorphous hydrogenated carbon. The experimental results show significant differences between the two coating series, where the films formed from C<sub>2</sub>H<sub>2</sub> exhibiting markedly superior characteristics in terms of microstructure, morphology, hardness, friction behaviour and wear resistance. For the coatings prepared using CH<sub>4</sub>, the measured values of crystallite size, hardness, friction coefficient and wear rate were in the ranges of 7.2–8.2 nm, 26–30 GPa, 0.3–0.4 and 2.1–4.8×10<sup>-6</sup> mm<sup>3</sup>N<sup>-1</sup>m<sup>-1</sup>, respectively, while for the coatings grown in C<sub>2</sub>H<sub>2</sub>, the values of these characteristics were found to be in the ranges of 3.1–3.7 nm, 41–45 GPa, 0.1–0.2 and 1.4–3.0×10<sup>-6</sup> mm<sup>3</sup>N<sup>-1</sup>m<sup>-1</sup>, respectively. Among the investigated coatings, that produced using C<sub>2</sub>H<sub>2</sub> at the highest flow rate (130 sccm) exhibited the highest hardness (45.1 GPa), the lowest friction coefficient (0.10) and the best wear resistance (wear rate of 1.4×10<sup>-6</sup> mm<sup>3</sup>N<sup>-1</sup>m<sup>-1</sup>).

Keywords: TiSiC-Cr coatings, cathodic arc, structure, mechanical properties, friction and wear

## 1. Introduction

The incorporation of different metals into amorphous hydrogenated carbon (a-C:H) films has been proved to be an effective method to reduce the residual compressive stress and consequently to improve film adhesion to metallic substrates [1–3]. Other beneficial effects of metal additions were found to be increased deposition rate, enhanced toughness, hardness, thermal stability, and modified electrical properties [1–13]. Such nanocomposite carbon based films (Me/a-C:H) containing pure metal (Me) or metal carbide (MeC) crystallites embedded in an a-C:H matrix generated great interest in various industrial applications within the last decade because of their superior characteristics such as chemical inertness, smooth surface morphology, high hardness, excellent lubricating properties and high resistance to wear [14–16]. Many of these films are considered as excellent candidates to provide long durability to the coated parts and components, mostly used in tribological applications. Various metals such as Ti, Zr, Nb, Ta, Cr, Mo, W, Ni, Co, Al, Ag or Cu having different affinities to carbon that determine peculiar chemical bonding states and structures, were taken into account, recently, as possible additives to a-C-H coating. The most known methods to produce these films are based on plasma assisted chemical vapor deposition, in which metallic elements are introduced by sputtering [4–7] or reactive magnetron sputtering [9,13,16], where the targets are made from the metals intended to be used as additives. Besides, ion beam assisted deposition [10,11,15] and cathodic arc evaporation [8,12] were also employed. Cathodic arc process was found to be a successful technique to also prepare other types of carbon containing films (e. g. doped a-SiC:H [17], graphene [18]). For both a-C:H [19–27] and Me/a-C:H [4,5] deposition, various hydrocarbon precursor gases such as CH<sub>4</sub>, C<sub>2</sub>H<sub>2</sub>, C<sub>2</sub>H<sub>4</sub>, C<sub>2</sub>H<sub>6</sub>, C<sub>4</sub>H<sub>10</sub> or C<sub>6</sub>H<sub>6</sub> were used. In these studies, the significant roles of the reactive gases, which are one of the key deposition parameters, on the structural, mechanical and tribological characteristics of films have been identified. Effects of other

gaseous environments (He, H<sub>2</sub>, N<sub>2</sub> etc.) on the properties of C-based coatings (a-C, a-C:H, a-C:N) have also been investigated [28–30].

The goal of this work was to investigate the effects of two carbon containing gases (CH<sub>4</sub> and C<sub>2</sub>H<sub>2</sub>) on the properties of TiSiC-Cr coatings, where Cr is an alloyed element to TiSiC basic compound. The selection of this coating was motivated by the increasing interest for TiSiC films which possess a combination of remarkable characteristics such as chemical stability, high hardness and strength, superior tribological performance, as well as good thermal and electrical conductivity [31–36]. The addition of small amounts of different metals to TiSiC has also been tested in the effort to improve the properties of these films [37–40]. In our previous works [38–40], we have examined the effects of alloying TiSiC with Zr, Cr or Ni by preparing them in CH<sub>4</sub> atmosphere. Among these investigated coatings, TiSiC-Zr was found to have the best tribological characteristics. In the case of TiSiC with Cr addition, it was found that its tribological performance under dry sliding conditions was rather poor [38]. In the present study, we show that the properties of the TiSiC-Cr film can be significantly enhanced, even beyond those of TiSiC-Zr, if C<sub>2</sub>H<sub>2</sub> is used as the carbon containing gas instead of CH<sub>4</sub>. Herein, the TiSiC-Cr coatings were produced by cathodic arc method under either CH<sub>4</sub> or C<sub>2</sub>H<sub>2</sub> hydrocarbon gas environment, where the deposition conditions were chosen to yield TiSiC-Cr coatings with high carbon contents (in excess of 50 at. %), so that these films can be considered as a-C:H coatings alloyed with Ti, Cr and Si in different concentrations, where Ti being the major alloying element. The films grown with both CH<sub>4</sub> and C<sub>2</sub>H<sub>2</sub> were fully characterized for their elemental and phase composition, chemical bonds, crystalline structure, cross-sectional morphology, mechanical properties and tribological performance. The role of hydrocarbon precursor gases (CH<sub>4</sub> and C<sub>2</sub>H<sub>2</sub>) in determining the properties of Me/a-C:H films is also discussed in detail.



## 2. Experimental procedure

The TiSiC-Cr coatings were prepared in a cathodic arc deposition unit equipped with two cathodes made of TiSi alloy (84 at. % Ti, 16 at. % Si; 99.9% purity) and Cr (99.9 % purity). Schematic of the deposition system is shown in Fig. 1. Two stainless steel grids were placed in front of the cathodes (at a distance of 10 cm) to reduce the number of macroparticles emitted by cathodes and deposited on substrate. The distances between the cathodes and substrate holder are also indicated in Fig. 1. The base pressure in the deposition chamber was typically in the  $10^{-4}$  Pa range. The substrates were ultrasonically cleaned with isopropanol (10 min) prior to the depositions and mounted on a rotating holder to ensure a homogeneous composition of the films. The samples were subsequently surface cleaned by sputter etching in Ar ( $10^{-1}$  Pa) through biasing for 10 min at -1000 V. Two series of coatings were prepared using either CH<sub>4</sub> (series-M) or C<sub>2</sub>H<sub>2</sub> (series-A) as reactive gases. For each series, three different gas flow rates ( $F_R$ ) were used (90, 110 and 130 sccm), corresponding to gas pressures of 1.9, 2.2 and  $2.5 \times 10^{-1}$  Pa, respectively. These values were chosen based on our previous findings [38] where a higher CH<sub>4</sub> flow rate of 150 sccm yielded films with rough surface morphology, due to the formation of agglomerated particles, which was proved to be detrimental to the tribological properties of the films. The resulting coatings were labelled M-90, M-110 and M-130 (for series-M) and A-90, A-110 and A-130 (for series-A). The arc currents were of 110 A and 100 A at TiSi and Cr cathodes, respectively. A negative bias voltage of -200 V was applied on the substrates, while the deposition temperature was of about 320 °C. The choice of -200 V for the substrate bias was made based on the preliminary experiments aimed to determine the best deposition conditions to prepare high hardness coatings. These experiments showed that the highest hardness was obtained for negative bias voltages in the range 180–220 V. As a temperature of ~320 °C was generated and maintained in the deposition chamber as a result of the substrate ion

bombardment and cathodes' thermal radiation, no additional substrate heating or cooling was used.

All coatings were deposited on three types of substrates such as (i) on 316 L stainless steel discs ( $\Phi$  20mm) for X-ray diffraction (XRD), (ii) on C 45 steel discs ( $\Phi$  25mm) for energy-dispersive X-ray spectroscopy (EDS), and for mechanical and tribological tests, and (iii) on Si (111) wafers ( $15 \times 15$  mm) for X-ray photoelectron spectroscopy (XPS), Raman spectroscopy (RS), elastic recoil detection analysis (ERDA) and scanning electron microscopy (SEM). Coatings with typical thicknesses of 3.6–3.9  $\mu\text{m}$  were prepared for XRD analysis by confining the deposition duration to 50–70 min.

Elemental compositions of the coatings were determined by energy-dispersive X-ray spectroscopy performed on a scanning electron microscope coupled with EDS (FEI Inspects equipment). The hydrogen content in the films were assessed by ERDA [41], performed using 2.537 MeV  $^4\text{He}^{++}$  particle beams from a 3.0 MV Tandem Van der Graaf accelerator. For ERDA measurements, the samples were placed on the sample holder at an angle of incidence of  $75^\circ$  with respect to the surface normal. The energy of recoiled particles was measured by an ORTEC silicon detector, placed at an exit angle of  $75^\circ$  with respect to the surface normal. A 3.2 mm diameter collimator was situated in front of this detector, resulting in a solid angle of 1.000 msr. To filter out the scattered helium ions mylar foils (11  $\mu\text{m}$  thick) were placed in front of the detector. Counting rates were always kept small enough in order to have a negligible dead time during the measurements. The chemical binding state was investigated by XPS and Raman spectroscopy. The XPS experiments were performed under ultra-high vacuum conditions ( $<2 \times 10^{-8}$  mbar) on a VG Scientific ESCA lab Mk II system, using Al  $K_\alpha$  radiation (1486.6 eV). An electron flood gun was used for charge compensation and the binding energy scale was referenced to the adventitious carbon 1s core-level at 284.8 eV. The analyser pass energy was set to 200 eV for the survey

spectrum, and 20 eV for individual core-level spectra. The sampling area was approximately 1 cm in diameter and the spectrometer resolution was 1.15 eV. The Raman spectra were collected in backscattering geometry using a LABRAM HR 800 instrument (Jobin -Yvon-France). An Ar<sup>+</sup> laser served as an excitation source at  $\lambda=488$  nm with a spot of 3  $\mu\text{m}$  diameter and a power of 5mW at the sample surface. XRD analysis was used to determine the crystalline structure, phase composition, texture and crystallite size (Rigaku Miniflex II diffractometer with CuK $\alpha$  radiation, operating in Bragg-Brentano configuration) of the films. The films cross-sectional morphologies were examined by nanoSAM Lab Scanning Auger Microscopy System (Omicron GmbH). Film thickness was measured using a Dektak 150 profilometer. Measurements of hardness were performed on a Vickers microhardness tester (0.05 N load). The coatings adhesion was determined by scratch tests under the conditions: indenter – 0.2 mm radius diamond stylus, load – continuous increase from 0 to 100 N, scratching speed –10 mm/min, scratching length – 10 mm. The critical load  $L_c$  was evaluated by optical examination of the scratch tracks.

In order to characterize the friction and wear behaviour of the coatings, tribological tests were conducted in dry atmosphere, using a CSM Instruments type ball-on-disc tribometer (sapphire ball of 6 mm diameter, 0.15 m/s sliding velocity, 300 m sliding distance, 5 N load). The worn volume was obtained by measuring the cross-sectional area of the wear track at 6 points of each track using the surface profiler. The worn surfaces were analyzed on the scanning electron microscope mentioned above.

All mechanical and tribological tests were conducted for each types of coatings on three specimens produced in the same batch, to ensure the testing reproducibility.

### 3. Results

#### 3.1. Elemental composition and chemical bonding structure

Film composition was determined using EDS (apart from hydrogen) and ERDA (for hydrogen content). The elemental compositions of the TiSiC-Cr coatings as obtained by EDS are summarized in Table 1, together with the C/(Ti+Cr) ratios. As seen, the Cr and Si contents are roughly similar in all the coatings, while carbon content is higher for the coatings deposited in C<sub>2</sub>H<sub>2</sub>, when using the same gas flow rate. Notably, the C/(Ti+Cr) ratio is higher than unity in all coatings, showing an increasing trend with gas flow rate.

A typical ERDA spectrum of hydrogen is shown in Fig. 2 (sample M-90). The hydrogen content in the deposited films as determined by ERDA (Table 1) is ranging from 0.5 to 1.1 at. % for series -M coatings and from 2.0 to 6.2 at. % for series -A, and increases with gas flow rate. This relative low H content is most likely due to the high ion bombardment of substrate [2] and to deposition temperature (~ 320 °C), both contributing to the loss of hydrogen.

The chemical bonding structure of the coatings was examined using XPS. The contaminants on the film surface (adventitious carbon, oxidized species) were removed by Ar<sup>+</sup> ion beam etching (4 keV, 5 min). Fig. 3 presents typical XPS survey spectra before and after sputter etching (sample M-90). As expected, the Ar<sup>+</sup> ion cleaning resulted in a significant reduction in the intensities of the peaks corresponding to the surface contaminants (O<sub>2</sub> and C), while the peaks corresponding to the metallic elements became more prominent. However, it is to be noted that a certain amount of oxygen is still present. This is in corroboration with a previous report (e.g. [42]) where a glow discharge optical spectroscopy (GDOS) experiments has shown the presence of oxygen in such films even at depths exceeding 100 nm.

Figs. 4 and 5 compare the Ti 2p, Cr 2p, Si 2p, and C1s XPS spectra after sputter etching for the samples M-90 and A-90, respectively. The peak assignment was done according to the literature data on Ti-based carbide coatings [13,31,33,35,40,43-48].

As can be observed in figures 4 and 5, the Ti, Cr and Si spectra of the coatings in the two series are not significantly different. The Ti  $2p_{3/2}$  peaks at 454.4–454.5, 455.2–455.3 and 457.3–457.8 eV can be attributed to Ti–C, Ti–C–O and Ti–O bonds, respectively; and Cr  $2p_{3/2}$  peaks at 574.6–574.7 and 577.3 eV to Cr–Cr/Cr–C and Cr–O bonds, respectively. In the case of Si, SiC compound and different Si oxidized species were identified at energies of 100.6–100.8 and 102.6–102.9 eV, respectively. It is apparent from the XPS spectra that the film contained various metals and Si oxidized species, in addition to the carbide compounds, that may be originated from the oxidization process during sample handling in open atmosphere.

The analysis of the carbon bonds was of special interest due to the major role played by the carbon binding state in determining the properties of the investigated coatings. For the sake of clarity, the XPS results comprising the identified carbon bonds, together with their relative amounts (% area), the corresponding binding energies, and the  $sp^2/sp^3$  ratios are summarized in Table 2.

It is worth mentioning that the XPS results show, for both coatings, the presence of a significant amount of free (hydrogenated) carbon phase ( $sp^2$  and  $sp^3$  bonds). The data in Table 2 also reveal the pronounced differences between the two types of coatings: for M–90, the C–C bonds have a relative area of 54.7 % (39.3 %  $sp^2$  and 15.4 %  $sp^3$ ), while for A–90 the relative area is of 77.5 % (67.7 %  $sp^2$  and 9.8 %  $sp^3$ ). As seen, the coating deposited with  $C_2H_2$  contains a higher amount of free carbon and a higher  $sp^2/sp^3$  ratio, indicating a more graphitic character of the carbon phase when using  $C_2H_2$  instead of  $CH_4$ .

The features found in the range 282.1–283.4 eV are difficult to be clearly indexed as the binding energies of C–Cr, C–Ti\* and C–Si bonds are located with small differences between them within this energy range and can not be clearly separated, as also reported for other types of complex metal carbides [43–45]. For example, based on some recently reported

studies on Ti-based carbides [33,35,43,44], the peaks at energies higher than 282.5 eV could partially be attributed to the occurrence of C–Ti\* bonds, which is assumed to be formed at the interface between the carbide crystalline grains and the amorphous carbon matrix. Specifically, in the case of M–90 and A–90 coatings, the carbon–metal (Si) bonds in the range of 281.6–283.4 eV are tentatively ascribed as follows. For M–90, the peak positioned at 281.6 eV is attributed to C–Ti bonds since  $281.6 \pm 0.2$  eV is the “standard” energy reported in most of the previous studies for this binding type [31,35,38,45]. The feature centred at 282.7 eV originates most likely from both the C–Cr and C–Ti\* bond contributions, influenced by the presence of Si in the bonding structure. In the case of the A–90 coating, similarly, the features at 282.1 and 283.4 eV were correlated with C–Ti and C–Cr/C–Ti\* bonds, respectively. According to this assignment, the binding energies in the case of A–90 sample appear to be shifted towards higher energies (with 0.5–0.7 eV). The observed shift could be related to the presence of oxygen in the region from where the XPS spectra were taken. Comparing the Ti 2p XPS spectra in Figs. 4 and 5 (B features), it appears that the relative amount of Ti–C–O oxidized species is higher for the A–90 coating. The presence of more oxygen generally leads to a shift to higher binding energies. Another possible explanation could be the reduction of the kinetic energy of the emitted photoelectrons as a result of the built-up of positive charge on the sample surface, which is more pronounced if surface is contaminated by more insulating/amorphous materials such as oxidized species. Carbon bonding structure was also examined using Raman spectroscopy. Fig. 6 shows representative RS spectra in the range  $1200\text{--}1750\text{ cm}^{-1}$  of the films prepared under CH<sub>4</sub> and C<sub>2</sub>H<sub>2</sub> gaseous environment (samples M–90 and A–90, respectively). As seen, the spectra are characterized by the presence of the peaks specific to disordered graphite: G – due to E<sub>2g</sub> mode of stretching vibrations of sp<sup>2</sup> atoms in rings and chains, and D – due to A<sub>1g</sub> breathing mode of sp<sup>2</sup> atoms in rings, activated by disorder. The most important RS parameters (G

position and intensity ratio  $I_D/I_G$ ) were obtained by peak deconvolution using a Gauss-Lorentz function and a linear function background (Table 3). The film prepared with  $C_2H_2$  exhibits a larger  $I_D/I_G$  ratio and a G peak position shifted towards higher wavenumbers when compared with the film grown in  $CH_4$ . According to the literature data [8,9,15,22,29,49], these results indicate a higher  $sp^2$  bonding content within the a-C:H phase for the A-90 film, and agree well with the earlier reported findings for a-C:H [22] and Me/a-C:H [5] films derived from  $CH_4$  and  $C_2H_2$ . The increased  $sp^2$  hybridization for the A-90 sample is consistent with the XPS results of the same samples (Table 2).

### 3.2. Crystalline structure and cross-sectional morphology

The X-ray diffraction patterns for all TiSiC-Cr films deposited on 316 L steel substrates are shown in Fig. 7, where striking differences between the coatings of the two series are observed. The diffractograms for the series-M coatings reveal the formation of a FCC solid solution with (220) preferred orientation. The coatings from series-A exhibit a lower degree of crystallinity, with a nearly random texture, low intensity and with wide (111), (200) and (220) peaks.

The observed structure and chemical composition of the coatings can be assigned to the role played by the amorphous hydrogenated carbon phase which is usually formed in carbide coatings with relatively high carbon content. As shown in numerous studies dedicated to multicomponent hard coatings (e.g. MeSiN, MeSiC, Me/a-C, Me/a-C:H), the presence of a segregated amorphous phase such as  $Si_3N_4$ , SiC, a:C etc. hinders the grain growth of the crystalline phase (MeN, MeC) [50,51]. This effect leads to a fine grain structure and an improvement of related mechanical and tribological properties (enhanced hardness and wear resistance, and reduced friction).

The crystallite sizes ( $d$ ) of the coatings, determined as a rough approximation using Scherrer formula [52], are given in Fig 7. It is to be noted that all coatings are nano-scale structured, having crystallite sizes of maximum 8.2 nm. In both series, the crystallite sizes vary within narrow ranges (7.2–8.2 nm for series –M, 3.1–3.7 nm for series –A), but there is a clear difference between the two series: the films of series –M have crystallite sizes almost double the size of those of series –A. This could be explained based on the different amounts of a-C:H environments present in the two cases, and also indirectly indicate the possible homogeneous distribution of these a-C:H phases.

The SEM cross-section images ( $\times 100,000$ ) of two representative samples prepared with  $\text{CH}_4$  and  $\text{C}_2\text{H}_2$  at a  $F_R$  of 90 sccm for 8 min are presented as Fig. 8a and 8b respectively, where the differences between the microstructures of the two films are clearly visible. As seen, the film in Fig. 8a exhibits a rough cross-section morphology. In contrast, the film deposited with  $\text{C}_2\text{H}_2$  (Fig. 8b) shows a much finer, practically featureless microstructure. This microstructural difference can be attributed to the presence of the higher proportion of the free carbon phase in the coatings of series –A as compared to series M, as also evidenced from the XPS data.

The smaller crystallite size and the finer microstructure observed for the series-A films could be attributed to the distribution of the a-C:H phase at the grain boundaries of the composite films. As the series-A films have more a-C:H phase, the distribution of them may be more homogeneous over all the grains thereby hindering the crystal growth more effectively.

### 3.3. Deposition rate and mechanical characteristics

The deposition rates and main mechanical characteristics of the TiSiC-Cr coatings (hardness and adhesion to C 45 steel substrates) are listed in Table 4. The deposition rates for the coatings of series –A were higher than those for the coatings of series –M, as also reported for DLC films prepared using  $\text{CH}_4$  and  $\text{C}_2\text{H}_2$  plasmas [24]. The increase of the deposition



rate ( $D_R$ ) values with increasing  $F_R$  value was also observed for both coating series. This increased deposition rate is consistent with the formation of more ionized as well as neutral species in  $C_2H_2$  atmosphere as compared to the  $CH_4$  environment ( $C_2H_2$  yields two carbon atoms instead of one atom by  $CH_4$ ).

The hardness (H) measurements presented a marked difference in hardness between the coatings deposited in  $CH_4$  and  $C_2H_2$ . The hardness values for the coatings of series–M range between about 26 GPa and 30 GPa, while the coatings of series–A show a significantly higher hardness values (H values are in the range 41–45 GPa). The materials with such high hardness values are normally classified as super-hard materials. This increase in hardness observed for the series-A films can partially be attributed to the grain boundary hardening phenomenon, as quantified by the Hall-Petch relationship:  $H \sim d^{-1/2}$  (H – hardness, d – grain size) [50]. From the H vs.  $d^{-1/2}$  plot presented in Fig. 9, it can be seen that the hardness values of the investigated coatings show a reasonable agreement with the Hall-Petch formula. The results of the adhesion measurements (Table 4) showed a satisfactory adhesion strength for the deposited films on the C 45 steel substrate, with measured critical loads ( $L_c$ ) ranging from ~21 to ~27 N. No significant differences between the critical loads of the two coatings types were observed.

#### 3.4. Tribological performance

The tribological tests were conducted on the TiSiC-Cr coated C45 steel discs. The tribological performance of the coatings was assessed by plotting the variation of the friction coefficient ( $\mu$ ) as a function of sliding distance (D) and by calculating the wear rate (k), defined as the worn volume (V) divided by the normal load (F) and the sliding distance (D):  $k = V/F \times D$ . The uncoated substrate was taken as reference. In order to identify the main

processes involved in the wear mechanism, the wear tracks morphology and composition were investigated using SEM and EDS.

The variation of the coefficient of friction versus sliding distance is presented in Fig. 10. For the uncoated sample, the friction coefficient is of approximately 0.55. For the TiSiC-Cr coatings, steady evolutions in time of the friction coefficient can be observed. The friction coefficients for the coatings of series–M show an increasing trend with sliding distance, while an almost constant  $\mu$  value is observed for the series–A coatings. It is also to be noted that the  $\mu$  values for the coatings prepared from  $C_2H_2$  are significantly lower than those for  $CH_4$ -derived coatings. It can also be seen from Fig. 10 that the friction coefficients for both the coating series decrease slightly with increasing gas flow rate, which can be attributed to the increase in the amount of the amorphous carbon phase, as presented in Table 2. The presence and concentration of the a:C-H phase determines the formation of a graphite-like transfer film in the sliding contact, with excellent lubricating properties, as currently reported in several publications (e.g. [35,53]).

Fig. 11 shows the values of the wear rate ( $k$ ) obtained from the ball-on-disc test for the investigated coatings, as well as for the uncoated substrate. As seen, wear rates ranging from  $1.4$  to  $4.8 \times 10^{-6} \text{ mm}^3 \text{ N}^{-1} \text{ m}^{-1}$  were measured. A slight decrease of the wear rate with increasing gas flow rate can be observed, the effect being more pronounced for the coatings of series–M. The highest wear resistance was found for the A–130 coating prepared with the highest flow rate of  $C_2H_2$ .

A detailed characterization of the wear tracks was conducted using the SEM and EDS analyses. Fig. 12 shows the SEM images of the wear tracks for selected samples (coatings from both series prepared at the lowest and highest  $F_R$ ).

The images taken at  $\times 100$  magnification (Fig. 12 a, c, e, g) reveal that the coatings grown in  $CH_4$  were markedly affected by the wear process. Within the wear track, a significant

amount of plastically deformed adhering material is observed. By contrast, for the coatings derived from  $C_2H_2$ , smooth surface morphologies are apparent. For both coating series, accumulation of wear debris along the two edges of the wear track can be seen. It should be also mentioned that by increasing the gas flow rate, the wear tracks become narrower, indicating an increased wear resistance.

The differences between the worn surfaces of the two coating series are more clearly evident at a higher magnification ( $\times 2000$ ; Fig. 12 b, d, f, h). For the series-M coatings, the adhering debris that builds up within the wear track are indicative of an adhesive wear. Besides, various defects (craters, scars) are observed on the worn surfaces. Also, zones with different shades of grey can be seen, suggesting changes in chemical composition of the film as a result of the wear process (probably oxidative phenomena, see below). In the case of the  $C_2H_2$  derived coatings, the worn surfaces differ sharply. The film surfaces appear to be smooth, with no scratches, fractures, cracks or plastic deformation being observed. It is interesting to note that although the coatings of series-M appear to be more affected by wear, the values of the wear rates for the two types of coatings are close. It seems that the material adhered to the worn surface hinders the continuous progress of the wear.

EDS analysis was performed in order to determine the dominant wear mechanism of the investigated coatings. The elemental compositions inside the wear tracks are given in Table 5. On comparing the atomic concentrations inside the wear tracks (Table 5) with those of the as-deposited films (Table 1), for the series-M coatings, significant changes in chemical compositions, precisely, a marked decrease in both metal and carbon concentrations are observed. These effects are accompanied by a corresponding increase in oxygen content, pointing to the major role played by the oxidation processes in the wear mechanism. Further, the presence of Fe (arising from the substrate) was detected in the EDS spectra at the worn zone of all these coatings, which also demonstrated a marked wear

damage for the coatings of series–M. Opposite conclusions can be drawn from the data for the TiSiC-Cr coatings prepared using  $C_2H_2$  (series-A; Table 5). The values of the atomic concentrations of the film components (Ti, Cr, Si, C) in the wear tracks are comparable to those for the film unaffected by the wear (Table 1). It can also be seen that Fe and O contents are relatively low, similar to the values measured for the as-deposited coatings. These findings demonstrate that the coatings suffered only minor wear damages, in agreement with the results from the SEM analysis.

To summarize, taking into account all the investigations performed, the TiSiC-Cr coatings produced in a  $C_2H_2$  atmosphere revealed a superior friction and wear behaviour when compared with the coatings deposited from  $CH_4$ . Combining the results of wear rate calculation, SEM examination and EDS analysis, the dominant wear mechanisms occurring for the coatings deposited with  $CH_4$  is identified to be involving an adhesive and oxidative wear, whereas the coatings with  $C_2H_2$  show a polishing wear mechanism.

#### 4. Discussion

The experimental results have demonstrated that the type of the carbon containing gas is one of the key deposition parameters which determine the properties of the TiSiC-Cr coatings. It is shown that the films prepared from  $C_2H_2$  are superior to those deposited with  $CH_4$  in terms of morphology, hardness and friction behaviour. It is worth emphasizing that the properties of metal alloyed a–C:H films depend on both the coexisting phases: crystalline phase (metal or metal carbide) and amorphous hydrogenated carbon, so that the results for alloyed a–C:H films can significantly differ from those of non-alloyed films. It appears that the film hardness and wear resistance for the TiSiC-Cr coatings resulted from the present study are mainly determined by the nanostructured carbide phase since, as shown above, the hardness behaviour obeys the Hall-Petch relationship that applies to nanocrystalline

materials [50]. The role of the a-C:H phase in the Hall-Petch mechanism is found to be indirect, through its influence on the crystallite development: the a-C:H phase existing in films prepared with C<sub>2</sub>H<sub>2</sub> hinders the grain growth to a greater extent compared to the films grown using CH<sub>4</sub>. In the case of non-alloyed a-C:H films, their hardness was found to be affected primarily by contents of hydrogen and sp<sup>3</sup> bonded carbon, and also by film density, all these being related to the energy of the species striking the growing film [20,21,25]. For example, the C<sub>2</sub>H<sub>x</sub> radicals condensed in C<sub>2</sub>H<sub>2</sub> plasmas are reported to form polymer chains as a result of the ion bombardment, leading to cross-linking and increasing sp<sup>3</sup> carbon bonds [5]. It is quite possible that such events may have also happened here to some extent and thus have affected the properties of the films investigated in the current study. On the other hand, it seems that the friction characteristics of the TiSiC-Cr coatings are controlled primarily by the amorphous carbon phase which works as a solid lubricant in the sliding contact, wherein the films with higher carbon content (those derived from C<sub>2</sub>H<sub>2</sub>) exhibit superior friction performance. These results are in contrast with those reported for a-C:H films without alloying elements [19], where it was shown that films prepared in C<sub>2</sub>H<sub>2</sub>, C<sub>2</sub>H<sub>4</sub>, C<sub>2</sub>H<sub>6</sub> and CH<sub>4</sub> exhibited better friction and wear performance with increasing H/C ratio (from C<sub>2</sub>H<sub>2</sub> to CH<sub>4</sub>).

Regarding the presence of hydrogen in film composition, it is commonly admitted that it plays an important role in the deposition process of the a-C:H films, significantly affecting their properties [2,49,54,55]. The presence of H influence the film growth and the nucleation process leading to formation of CH<sub>x</sub> and C<sub>2</sub>H<sub>x</sub> clusters, increase the sp<sup>3</sup> content by saturating the C=C bonds with H, stabilize the diamond clusters, preferentially sputter the sp<sup>2</sup> carbon and passivate the film surfaces. In the case of our films, the hydrogen content, as resulted from ERDA measurements, is relatively low, ranging from 0.5 to 6.2 at. %. According to Ferrari [54], for a low H content of < 20 at. % the hydrogen introduction in a mainly sp<sup>2</sup>

carbon induces both disordering and ordering effects which tend to compensate each other. However, it is not excluded that hydrogen would influence the properties of the films under investigation in this work, particularly their friction characteristics. For example, the A-130 film, having the highest H content, revealed a significantly better friction performance and this could be the result of the combining effects of both graphite-like carbon and hydrogen contents. As commonly admitted, the presence of hydrogen leads to a reduction in the adhesive component of wear-friction mechanism as a result of the passivation of the surface dangling carbon bonds (e. g. [3,19]). At present, the effects of H content are difficult to be distinguished from those of other factors.

It is also important to mention that in the existing studies focused on the precursor gas effect on the structure and properties of the a-C:H films with or without metal addition, different processing parameters were considered as experimental variables. For non-alloyed films, such variables considered were reactive gas flow rate [26,27], ratio of hydrocarbon to total gas flow [25], discharge power [24], substrate bias voltage [22,27], substrate current [27] or  $V_s/p^{1/2}$  ratio ( $V_s$  – substrate bias,  $p$  – deposition pressure) [21]. The films were mostly deposited by (microwave or RF) PACVD techniques and the tested source gases were  $\text{CH}_4$  and  $\text{C}_2\text{H}_2$  [24],  $\text{CH}_4$  and  $\text{C}_6\text{H}_6$  [21],  $\text{C}_2\text{H}_2$  and  $\text{C}_2\text{H}_4$  [26],  $\text{C}_2\text{H}_2$  and  $\text{C}_4\text{H}_{10}$  [25,27],  $\text{CH}_4$ ,  $\text{C}_2\text{H}_6$ ,  $\text{C}_2\text{H}_4$  and  $\text{C}_2\text{H}_2$ [19],  $\text{CH}_4+\text{Ar}$  and  $\text{C}_2\text{H}_2+\text{Ar}$  [22]. The influence of the precursor gas on the film characteristics was evaluated by a comparative film examination at similar values of the above mentioned deposition parameters. In the case of metal alloyed films (Cu/a-C:H) [5,8], grown by combined microwave PACVD and sputtering in  $\text{CH}_4+\text{Ar}$  mixtures, the experimental variable was the concentration of hydrocarbon in the gas phase and the films were comparatively investigated for similar carbon contents in the film. For the present study, the hydrocarbon ( $\text{CH}_4$  or  $\text{C}_2\text{H}_2$ ) flow rate was taken as the variable process parameter, while arc currents, substrate bias and substrate temperature were kept constant. Under these

conditions, it was found that for the same value of flow rate the films grown from  $C_2H_2$  possessed a significantly higher carbon content as compared to the  $CH_4$  derived films. Therefore, at first sight, the significant difference between the properties of the two coating types could be explained by simply assuming that the amount of the free hydrogenated carbon phase dictates the coating properties. This assumption is also supported by the fact that, for the same reactive gas, film characteristics improved with increasing carbon content. However, this does not entirely explain the results of the experiments. For example, if we examine two coatings with comparable values of carbon contents but prepared from  $CH_4$  and  $C_2H_2$  at different flow rates (samples M-130 and A-90, with carbon contents of ~ 57 and 59 at. %, respectively), marked differences are still present (sample A-90 has finer microstructure, higher hardness and superior friction performance). As a consequence, it is reasonable to consider that the peculiarities of the film chemical characteristics (hydrogen content, chemical bonds) and of the hydrogenated carbon phase (carbon configuration – clusters, chains, rings –, bonding structure,  $sp^3/sp^2$  carbon bond ratio, space distribution) influence the properties of the coatings. Depending on the carbon containing gas, different ionized and neutral species were identified in the plasma environment [4]. The radicals formed in the plasma condense on the substrate surface and are considered to play a significant role in the growth mechanism of the film [4]. For example, in  $CH_4$  plasmas, the major neutral species are  $CH_x$  radicals, while the  $C_2H_2$  environment contains mainly  $C_2H_x$  radicals and this can cause differences in film properties, particularly in the growth of crystallites (dimensions, distance between crystallites) [4]. Therefore, in order to clarify all the aspects regarding the effects of precursor gas on TiSiC-Cr coating characteristics, a more detailed and deeper insight into the microchemical and microstructural properties of the films are required, which are currently being performed and will be communicated separately.

## 5. Conclusions

TiSiC-Cr nanocomposite coatings were prepared by a cathodic arc method using either CH<sub>4</sub> or C<sub>2</sub>H<sub>2</sub> as reactive gases. The coatings, with carbon/metal ratios higher than unity (1.3–2.9), consisted of a mixture of crystalline solid solution carbide and amorphous hydrogenated carbon phases.

It was found that the coatings derived from C<sub>2</sub>H<sub>2</sub> outperformed those prepared in CH<sub>4</sub> plasma in all of the relevant film characteristics (microstructure, hardness, friction and wear performance). The findings suggest that the source gas type should be considered as a key experimental parameter in addition to the gas pressure, cathode current and the substrate bias voltage. The experimental results demonstrate the significant role of the hydrogenated carbon phase played in determining the properties of the coatings, wherein the films deposited in C<sub>2</sub>H<sub>2</sub> atmosphere showing a significantly higher carbon content and hence superior properties.

Importantly, a state of superhardness was achieved ( $H > 40$  GPa) for the Cr – alloyed TiSiC coatings when C<sub>2</sub>H<sub>2</sub> was employed as the precursor gas. Further for both the coating types, hardness, friction and the wear characteristics were improved with increasing the reactive gas flow rate (or carbon content). For the coatings deposited from CH<sub>4</sub>, adhesive and oxidative processes were found to be dominant in the wear mechanism, while for those prepared from C<sub>2</sub>H<sub>2</sub>, a mild polishing wear was observed. A higher concentration of a-C:H phase, and their possible homogeneous distribution around the grain boundaries are proposed as the main reason for the significant enhancement of the overall properties.



## Acknowledgements

Work supported under the Grant of the Romanian National Authority for Scientific Research (CNCS – UEFISCDI), projects no. PN-II-PT-PCCA-2011-3.2-1453 and no. PN-II-ID-PCE-2011-3-1016. SCP and MAM would like to thank Enterprise Ireland (CF/2014/4370) and the AMBER Research Centre (12/RC/2278) respectively for the financial support.

## References

- [1] J.C. Sánchez-López, A. Fernández, Doping and alloying effects on DLC coatings, in: C. Donnet, A. Erdemir (Eds.), *Tribology Diamond-like Carbon Films*, Springer Science, New York, 2008, pp. 311–328.
- [2] J. Robertson, Classification of diamond-like carbons, in: C. Donnet, A. Erdemir (Eds.), *Tribology Diamond-like Carbon Films*, Springer Science, New York, 2008, pp. 13–24.
- [3] K.P. Furlan, A.N. Klein, D. Hotza, Diamond-like carbon films deposited by hydrocarbon plasma sources, *Rev. Adv. Mater. Sci.* 34 (2013) 165–172.
- [4] F. Thiéry, Y. Pauleau, J.J. Grob, D. Babonneau, Structural characteristics of copper/hydrogenated amorphous carbon composite films prepared by microwave plasma-assisted deposition processes from methane–argon and acetylene–argon gas mixtures, *Thin Solid Films* 466 (2004) 10–15.
- [5] V.V. Uglov, A.K. Kuleshov, M.V. Astashynskaya, V.M. Anishchik, S.N. Dub, F. Thiery, Y. Pauleau, Mechanical properties of copper/carbon nanocomposite films formed by microwave plasma assisted deposition techniques from argon-methane and argon-acetylene gas mixtures, *Compos. Sci. Technol.* 65 (2005) 785–791.
- [6] S. Kucielka, W. Gulbiński, Y. Pauleau, S.N. Dub, J.J. Grob, Composition, mechanical properties and friction behavior of nickel/hydrogenated amorphous carbon composite films, *Surf. Coat. Technol.* 200 (2006) 6258–6262.
- [7] Y. Pauleau, V.V. Uglov, A.K. Kuleshov, M.V. Astashynskaya, M.P. Samtsov, S.N. Dub, Structure and mechanical properties of nickel/carbon nanocomposite films formed by microwave plasma-assisted deposition technique from argon–acetylene gas

- mixture, *Surf. Coat. Technol.* 202 (2008) 2282–2286.
- [8] R.K.Y. Fu, Y.F. Mei, M.Y. Fu, X.Y. Liu, P.K. Chu, Thermal stability of metal-doped diamond-like carbon fabricated by dual plasma deposition, *Diam. Relat. Mater.* 14 (2005) 1489–1493.
- [9] G. Gassner, P.H. Mayrhofer, C. Mitterer, J. Kiefer, Structure–property relations in Cr–C/a-C:H coatings deposited by reactive magnetron sputtering, *Surf. Coat. Technol.* 200 (2005) 1147–1150.
- [10] K. Baba, R. Hatada, Preparation and properties of metal-containing diamond-like carbon films by magnetron plasma source ion implantation, *Surf. Coat. Technol.* 196 (2005) 207–210.
- [11] K. Baba, R. Hatada, Y. Tanaka, Preparation and properties of W-containing diamond-like carbon films by magnetron plasma source ion implantation, *Surf. Coat. Technol.* 201 (2007) 8362–8365.
- [12] W. Gou, X. Chu, G. Li, Structure and properties of Cr-containing hydrogenated amorphous carbon films synthesized by filtered cathodic vacuum arc system, *Plasma Process. Polym.* 4 (2007) 269–272.
- [13] I. Bertóti, A. Tóth, M. Mohai, J. Szépvölgyi, Chemical structure and mechanical properties of Si-containing a-C:H and a-C thin films and their Cr- and W-containing derivatives, *Surf. Coat. Technol.* 206 (2011) 630–639.
- [14] G.J. Van Der Kolk, Wear resistance of amorphous DLC and metal containing DLC in industrial applications, in: *Tribology Diamond-Like Carbon Film*, Springer Science, New York, 2008, pp. 484–493.
- [15] J.L. Endrino, R. Escobar Galindo, H.-S. Zhang, M. Allen, R. Gago, A. Espinosa, A.

- Anders, Structure and properties of silver-containing a-C(H) films deposited by plasma immersion ion implantation, *Surf. Coat. Technol.* 202 (2008) 3675–3682.
- [16] A. Escudeiro, T. Polcar, A. Cavaleiro, a-C(:H) and a-C(:H)\_Zr coatings deposited on biomedical Ti-based substrates: Tribological properties, *Thin Solid Films* 538 (2013) 89–96.
- [17] R.K. Tripathi, O.S. Panwar, A.K. Kesarwani, I. Rawal, B.P. Singh, M.K. Dalai, S. Chockalingam, Investigations on phosphorous doped hydrogenated amorphous silicon carbide thin films deposited by a filtered cathodic vacuum arc technique for photo detecting applications, *RSC Adv.* 4 (2014) 54388–54397.
- [18] O.S. Panwar, A.K. Kesarwani, S.R. Dhakate, B.P. Singh, R.K. Rakshit, A. Bisht, S. Chockalingam, Few layer graphene synthesized by filtered cathodic vacuum arc technique, *J. Vac. Sci. Technol. B* 31 (2013) 040602.
- [19] A. Erdemir, I.B. Nilufer, O.L. Eryilmaz, M. Beschliesser, G.R. Fenske, Friction and wear performance of diamond-like carbon films grown in various source gas plasmas, *Surf. Coat. Technol.* 120–121 (1999) 589–593.
- [20] D. Sarangi, O.S. Panwar, S. Kumar, R. Bhattacharyya, Characterization studies of diamond-like carbon films grown using a saddle-field fast-atom-beam source, *J. Vac. Sci. Technol. A Vacuum, Surfaces, Film* 18 (2000) 2302
- [21] K.-R. Lee, Y.-J. Baik, K.Y. Eun, S. Han, Precursor gas effect on the structure and properties of diamond-like carbon films, *Diam. Relat. Mater.* 3 (1994) 1230–1234.
- [22] K.H. Lai, C.Y. Chan, M.K. Fung, I. Bello, C.S. Lee, S.T. Lee, Mechanical properties of DLC films prepared in acetylene and methane plasmas using electron cyclotron resonance microwave plasma chemical vapor deposition, *Diam. Relat. Mater.* 10 (2001) 1862–1867.

- [23] M. Yoshida, S. Watanabe, T. Tanaka, T. Takagi, M. Shinohara, J.W. Lee, Investigation of diamond-like carbon formed on PET film by plasma-source ion implantation using  $C_2H_2$  and  $CH_4$ , *Nucl. Instruments Methods Phys. Res. Sect. B Beam Interact. with Mater. Atoms.* 206 (2003) 712–716.
- [24] M.K. Hassan, B.K. Pramanik, A. Hatta, Electrical resistivities of the diamond-like carbon films fabricated from methane and acetylene using RF plasma, *New Diam. Front. Carbon Technol.* 16 (2006) 211–219.
- [25] J.M. Lackner, R. Major, L. Major, T. Schöberl, W. Waldhauser, RF deposition of soft hydrogenated amorphous carbon coatings for adhesive interfaces on highly elastic polymer materials, *Surf. Coat. Technol.* 203 (2009) 2243–2248.
- [26] C.P. Chen, A.H. Tan, Characterisation and microcorrosion of DLC ultrathin films with acetylene and ethylene source gases by PECVD, *Surf. Eng.* 27 (2011) 151–157.
- [27] J. Wöckel, B. Dzur, J. Emmerlich, M. Müller, S. Rath, D. Spreemann, Influence of the precursor gas on the process and layer properties of DLC films, in: 22nd International Symposium on Plasma Chemistry, Antwerp, Belgium, n.d.: pp. P–III–6–54.
- [28] O.S. Panwar, M.A. Khan, G. Bhagavanarayana, P.N. Dixit, S. Kumar, C.M.S. Rauthan, Effect of hydrogen and nitrogen incorporation on the properties of tetrahedral amorphous carbon films grown using S bend filtered cathodic arc process, *Indian J. Pure Appl. Phys.* 46 (2008) 797–805.
- [29] Ishpal, O.S. Panwar, M. Kumar, S. Kumar, Effect of ambient gaseous environment on the properties of amorphous carbon thin films, *Mater. Chem. Phys.* 125 (2011) 558–567.

- [30] O.S. Panwar, R.K. Tripathi, S. Chockalingam, Improved nanomechanical properties of hydrogenated tetrahedral amorphous carbon films measured with ultra low indentation load, *Mater. Express* 5 (2015) 410–418.
- [31] P. Eklund, J. Emmerlich, H. Högberg, O. Wilhelmsson, P. Isberg, J. Birch, P.O.Å. Persson, U. Jansson, L. Hultman, Structural, electrical, and mechanical properties of nc-TiC/a-SiC nanocomposite thin films, *J. Vac. Sci. Technol. B Microelectron. Nanom. Struct.* 23 (2005) 2486.
- [32] M. Rester, J. Neidhardt, P. Eklund, J. Emmerlich, H. Ljungcrantz, L. Hultman, C. Mitterer, Annealing studies of nanocomposite Ti-Si-C thin films with respect to phase stability and tribological performance, *Mater. Sci. Eng. A.* 429 (2006) 90–95.
- [33] J. Lauridsen, P. Eklund, T. Joelsson, H. Ljungcrantz, Å. Öberg, E. Lewin, U. Jansson, M. Beckers, H. Högberg, L. Hultman, High-rate deposition of amorphous and nanocomposite Ti–Si–C multifunctional coatings, *Surf. Coat. Technol.* 205 (2010) 299–305.
- [34] C. Lopes, N.M.G. Parreira, S. Carvalho, A. Cavaleiro, J.P. Rivière, E. Le Bourhis, F. Vaz, Magnetron sputtered Ti–Si–C thin films prepared at low temperatures, *Surf. Coat. Technol.* 201 (2007) 7180–7186.
- [35] J. Jiang, J. Hao, X. Pang, P. Wang, W. Liu, Structure and characteristics of amorphous (Ti,Si)-C:H films deposited by reactive magnetron sputtering, *Diam. Relat. Mater.* 19 (2010) 1172–1177.
- [36] H.W. Strauss, R.R. Chromik, S. Hassani, J.E. Klemberg-Sapieha, In situ tribology of nanocomposite Ti–Si–C–H coatings prepared by PE-CVD, *Wear.* 272 (2011) 133–148.

- [37] P. Eklund, T. Joelsson, H. Ljungcrantz, O. Wilhelmsson, Z. Czigány, H. Högberg, L. Hultman, Microstructure and electrical properties of Ti–Si–C–Ag nanocomposite thin films, *Surf. Coat. Technol.* 201 (2007) 6465–6469.
- [38] C. Vitelaru, M. Balaceanu, A. Parau, C.R. Luculescu, A. Vladescu, Investigation of nanostructured TiSiC–Zr and TiSiC–Cr hard coatings for industrial applications, *Surf. Coat. Technol.* 251 (2014) 21–28.
- [39] A.C. Parau, C. Vitelaru, M. Balaceanu, V. Braic, L.R. Constantin, M. Braic, A. Vladescu, TiSiC, TiSiC-Zr, and TiSiC-Cr Coatings—Corrosion Resistance and Tribological Performance in Saline Solution, *Tribol. Trans.* 59 (2016) 72–79.
- [40] M. Balaceanu, A.C. Parau, M. Braic, A. Vladescu, C.R. Luculescu, C. Logofatu, V. Braic, Growth and characterization of arc evaporated TiSiC-Ni coatings, *Tribol. Lett.* 58 (2015) 1–9.
- [41] Handbook of Modern Ion Beam Materials Analysis, 2nd ed., Y. Wang, M. Nastasi (Eds), Published: March 2010.
- [42] M. Balaceanu, V. Braic, A. Kiss, C.N. Zoita, A. Vladescu, M. Braic, I. Tudor, A. Popescu, R. Ripeanu, C. Logofatu, C.C. Negriila, Characteristics of arc plasma deposited TiAlZrCN coatings, *Surf. Coat. Technology* 202 (2008) 3981–3987
- [43] E. Lewin, P.O.Å. Persson, M. Lattemann, M. Stüber, M. Gorgoi, A. Sandell, C. Ziebert, F. Schäfers, W. Braun, J. Halbritter, S. Ulrich, W. Eberhardt, L. Hultman, H. Siegbahn, S. Svensson, U. Jansson, On the origin of a third spectral component of C1s XPS-spectra for nc-TiC/a-C nanocomposite thin films, *Surf. Coat. Technol.* 202 (2008) 3563–3570.
- [44] E. Lewin, M. Gorgoi, F. Schäfers, S. Svensson, U. Jansson, Influence of sputter damage on the XPS analysis of metastable nanocomposite coatings, *Surf. Coat.*

- Technol. 204 (2009) 455–462.
- [45] U. Jansson, E. Lewin, M. Råsander, O. Eriksson, B. André, U. Wiklund, Design of carbide-based nanocomposite thin films by selective alloying, *Surf. Coat. Technol.* 206 (2011) 583–590.
- [46] O. Tengstrand, N. Nedfors, B. Alling, U. Jansson, A. Flink, P. Eklund, L. Hultman, Incorporation effects of Si in TiC<sub>x</sub> thin films, *Surf. Coat. Technol.* 258 (2014) 392–397.
- [47] B. Crist, *Handbook of monochromatic XPS spectra*, XPS International LLC, Mountain View CA, 2004.
- [48] M. Braic, V. Braic, M. Balaceanu, A. Vladescu, C.N. Zoita, C.P. Lungu, C.E.A. Grigorescu, E. Grigore, C. Logofatu, (Ti,Cr,Nb)CN coatings deposited on nitrided high-speed steel by cathodic arc method, *Surf. Coat. Technol.* 205 (2011) S209–S213.
- [49] A. Ferrari, J. Robertson, Interpretation of Raman spectra of disordered and amorphous carbon, *Phys. Rev. B.* 61 (2000) 14095–14107.
- [50] S. Vepřek, The search for novel, superhard materials, *J. Vac. Sci. Technol. A Vacuum, Surfaces, Film.* 17 (1999) 2401.
- [51] J. Musil, Properties of hard nanocomposite thin films, in: S. Zhang, N. Ali (Eds.), *Nanocomposite Thin Film. Coatings*, Published by Imperial College Press and distributed by World Scientific Publishing CO., London, 2007, pp. 281–328.
- [52] P. Scherrer, Bestimmung der Grösse und der Inneren Struktur von Kolloidteilchen Mittels Röntgenstrahlen, *Nachr. Ges. Wiss. Göttingen*, 26 (1918) 98 – 100.
- [53] C. Mitterer, N. Fateh, F. Munnik, Microstructure-property relations of reactively



- magnetron sputtered  $VC_xN_y$  films, *Surf. Coat. Technol.* 205 (2011) 3805–3809.
- [54] Andreea C. Ferrari, Non-destructive characterisation of carbon films, in: C. Donnet, A. Erdemir (Eds.), *Tribology Diamond-like Carbon Film*, Springer Science, New York, 2008: pp. 49.
- [55] S. Michaelson, Y. Lifshitz, O. Ternyak, R. Akhvlediani, A. Hoffman, Hydrogen incorporation in diamond films, *Diam. Relat. Mater.* 16 (2007) 845–850.

**Figures caption:**

Fig. 1. Schematic of the deposition chamber ( $d_1 = 500$  mm,  $d_2 = 300$  mm and  $d_3 = 80$  mm)

Fig. 2. ERDA spectrum of hydrogen for the M-90 coating

Fig. 3. Typical XPS survey spectra before and after sputter etching (M-90 coating)

Fig. 4. XPS Ti 2p, Cr 2p, Si 2p and C 1s spectra of the M-90 coating after sputter etching

Fig. 5. XPS Ti 2p, Cr 2p, Si 2p and C 1s spectra of the A-90 coating after sputter etching

Fig. 6. Raman spectra of the M-90 and A-90 coatings

Fig. 7. X-ray diffraction patterns of TiSiC-Cr coatings deposited on 316 L substrates

(s – substrate; d – crystallite size)

Fig. 8. SEM cross-section images ( $\times 100,000$ ) of the M-90 (a) and A-90 (b) coatings

Fig. 9. Hardness (H) as a function of inverse square root of the grain size (d)

Fig. 10. Plots of the coefficient of friction ( $\mu$ ) as a function of sliding distance (D) for the uncoated substrate and TiSiC-Cr coatings (dry testing conditions; sapphire ball, 0.15 m/s, 300 m sliding distance, 5 N load)

Fig. 11. Wear rate (k) for the TiSiC-Cr coatings and the substrate (C 45 steel)

Fig. 12. SEM micrographs, at two magnifications, of the wear tracks for the TiSiC-Cr coatings (a): M-90 ( $\times 100$ ), (b): M-90 ( $\times 2000$ ), (c): M-130 ( $\times 100$ ), (d): M-130 ( $\times 2000$ ), (e): A-90 ( $\times 100$ ), (f): A-90 ( $\times 2000$ ), (g): A-130 ( $\times 100$ ), (h): A-130 ( $\times 2000$ ) (the SEM images at  $\times 2000$  and the EDS analyses were performed within the circled areas)

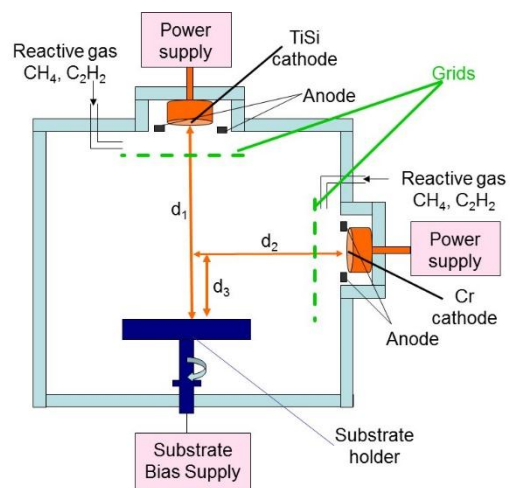


Fig. 1

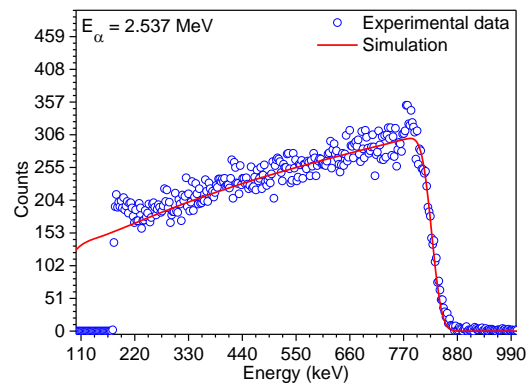


Fig. 2

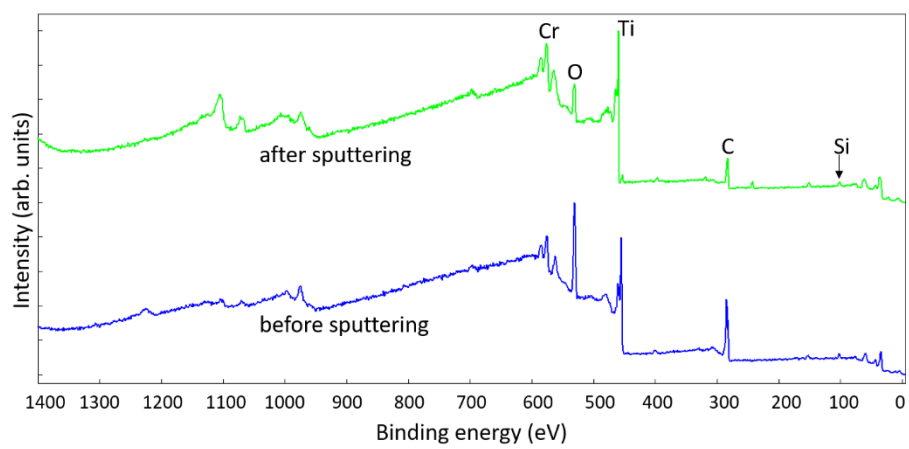


Fig. 3

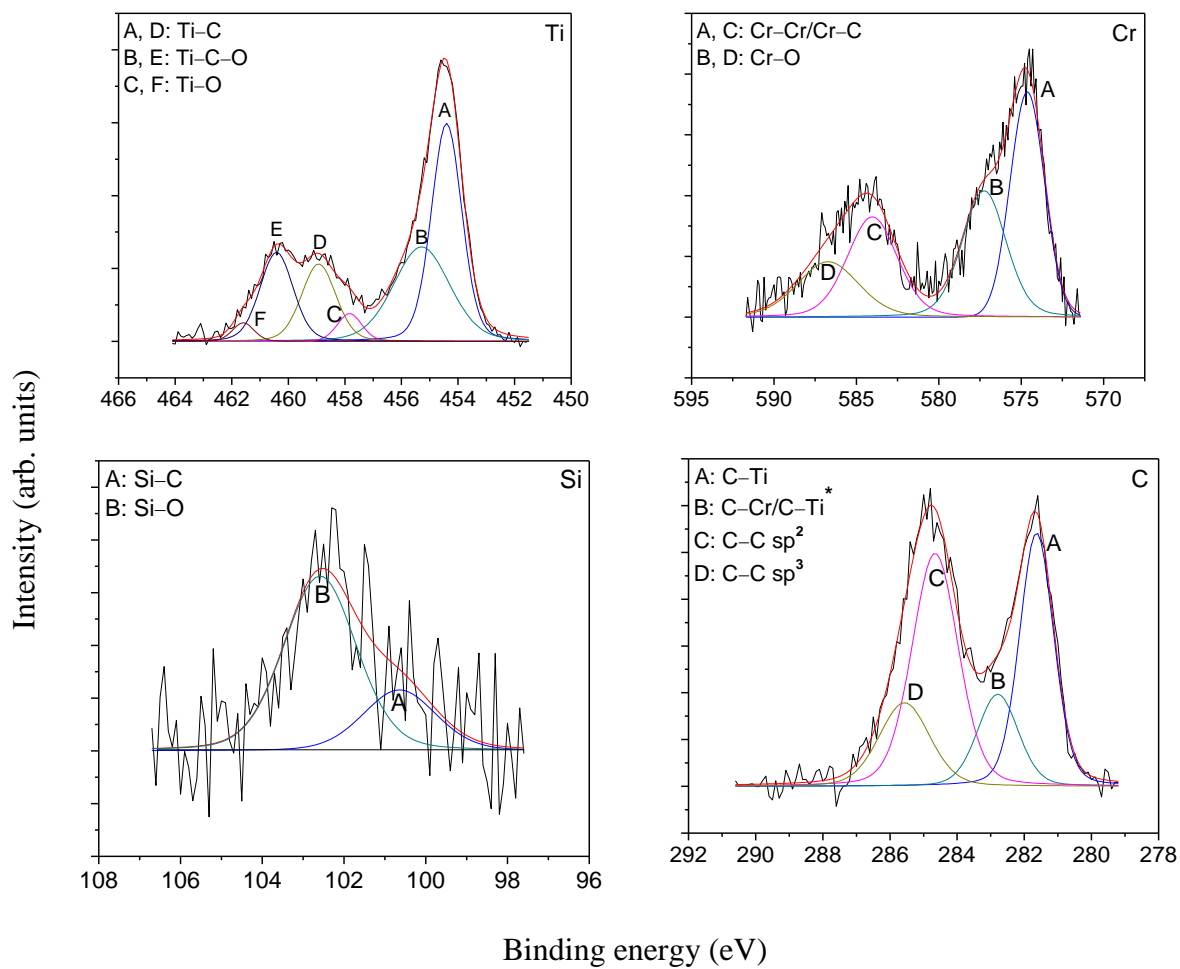


Fig. 4

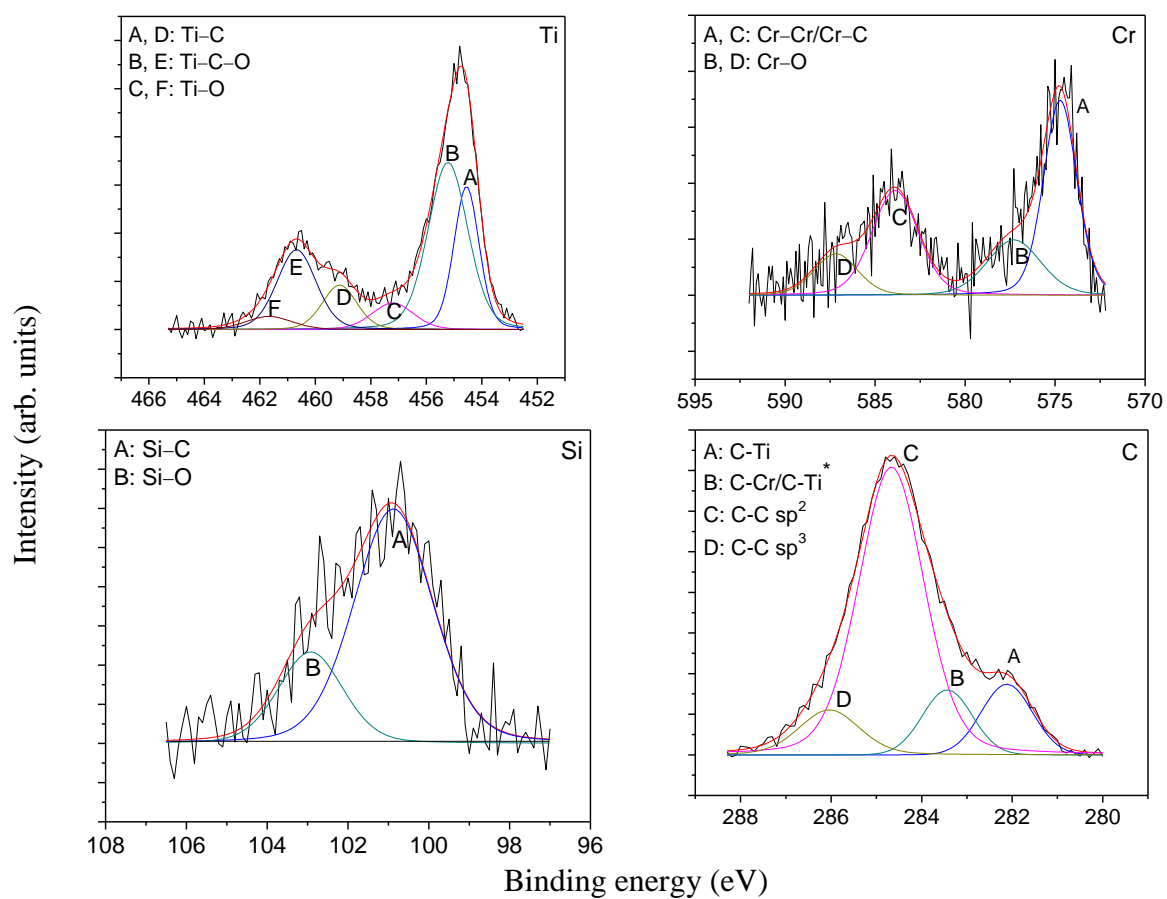


Fig. 5

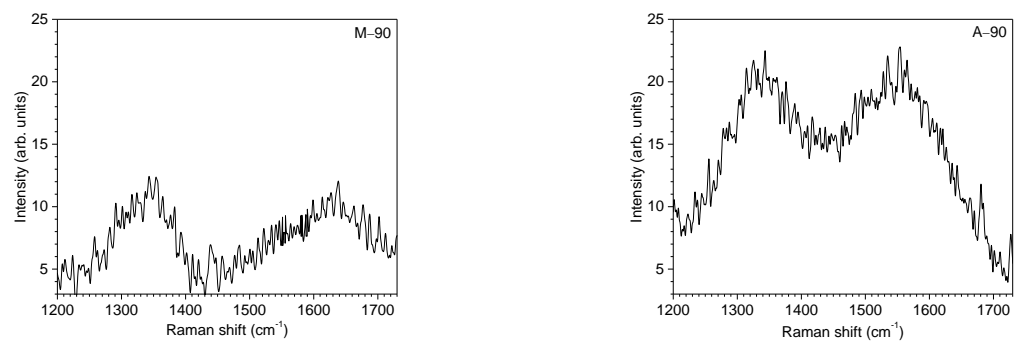


Fig. 6



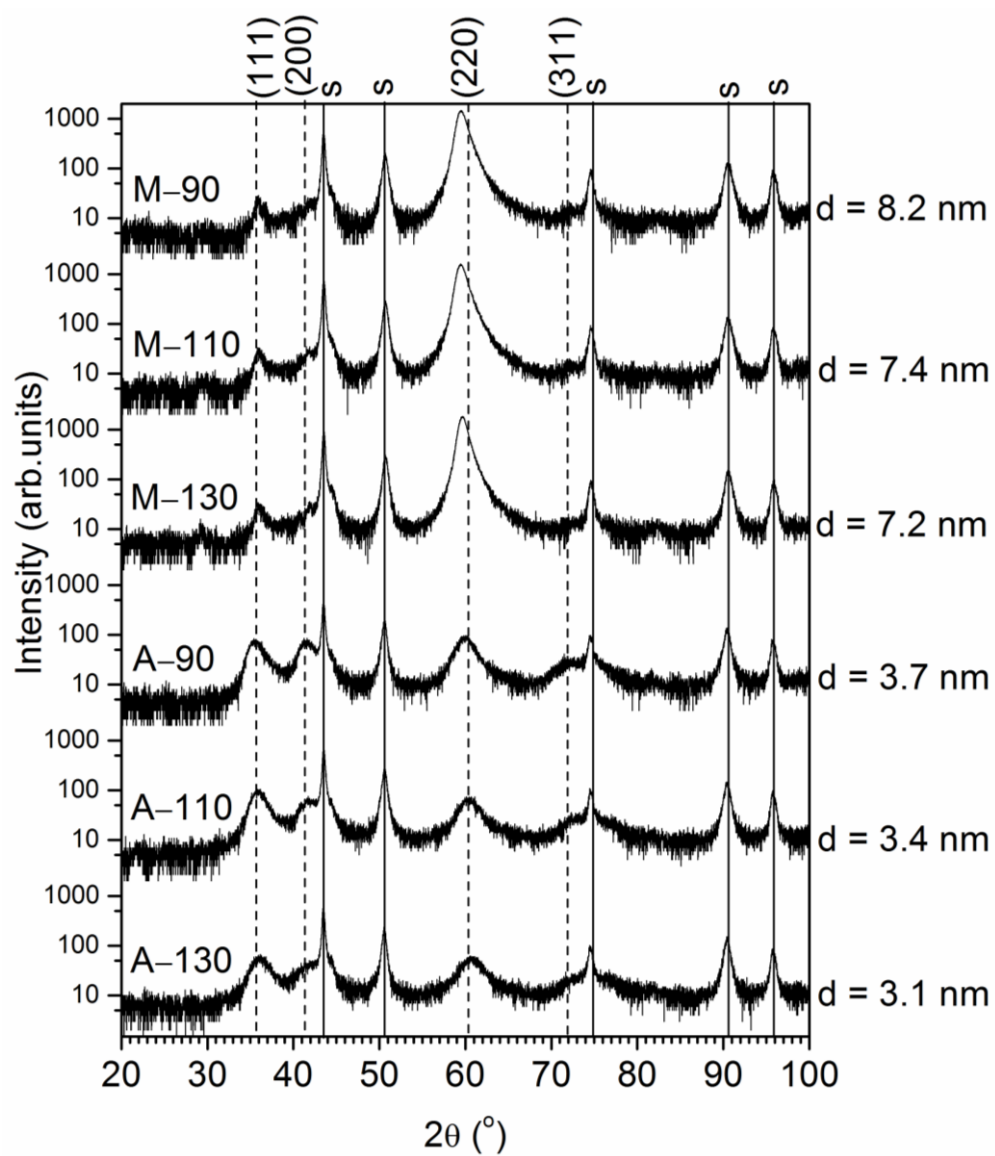


Fig. 7

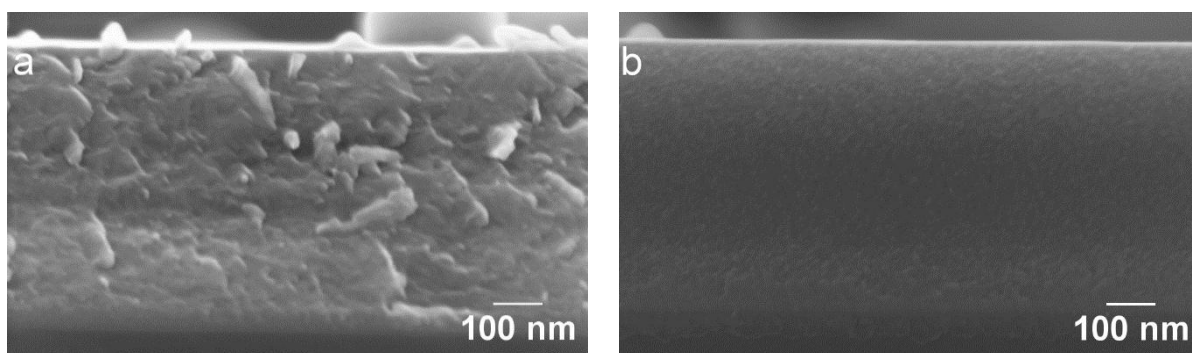


Fig. 8

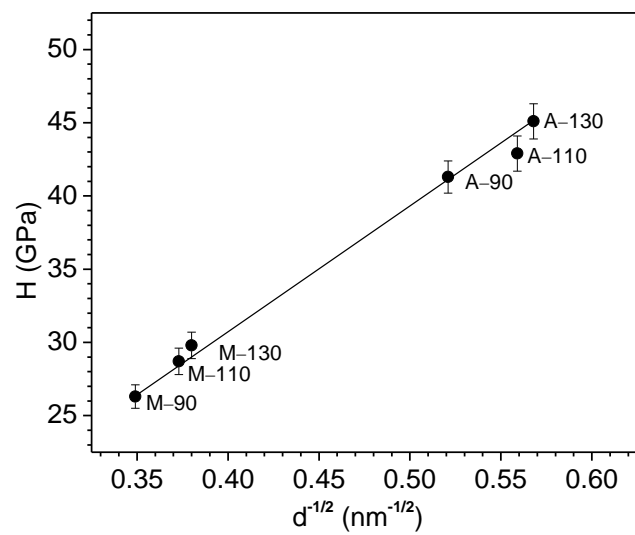


Fig. 9

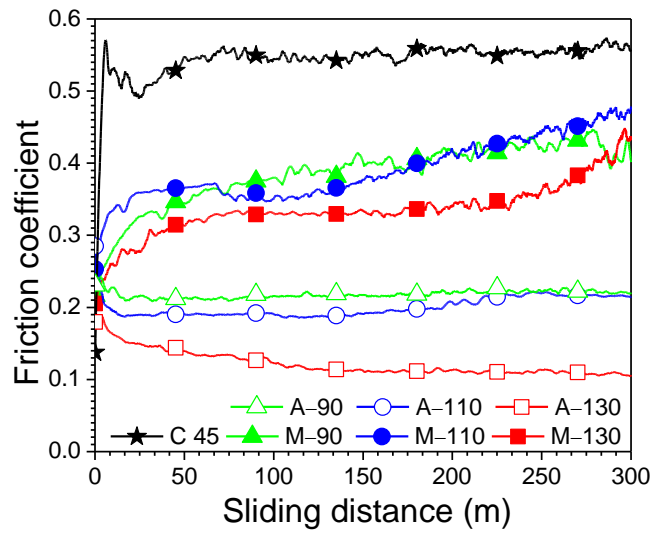


Fig. 10

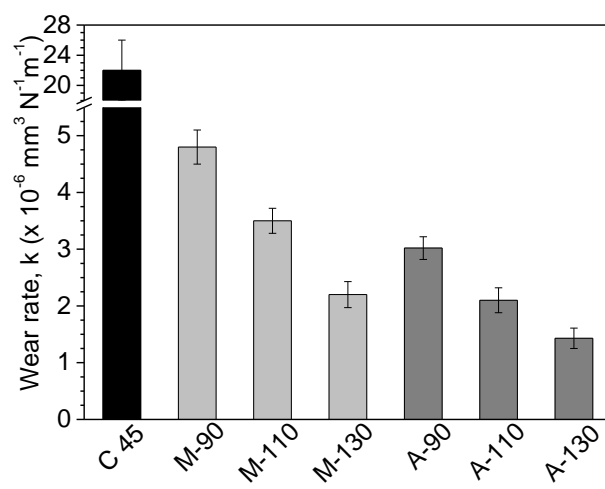


Fig. 11

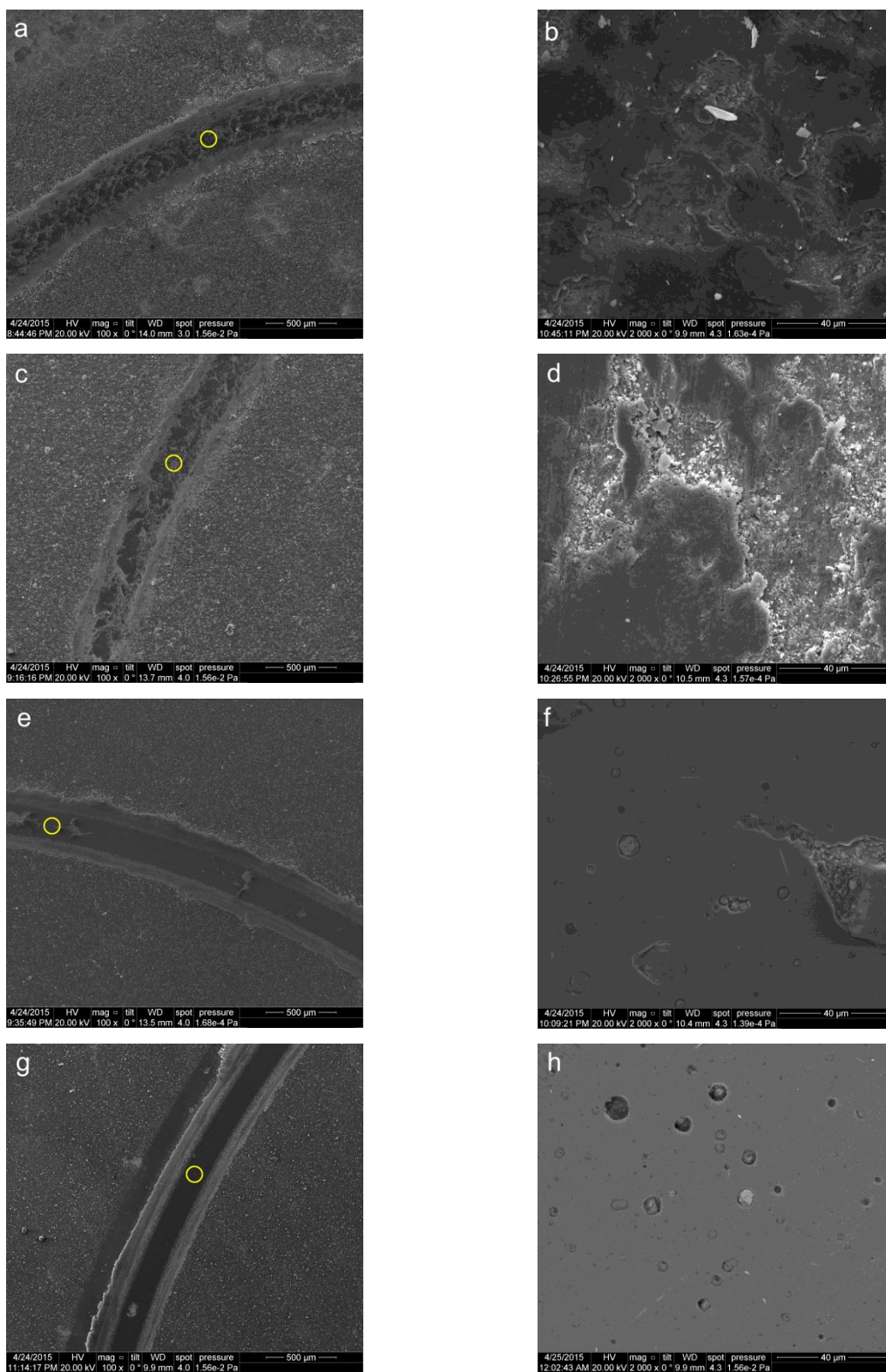


Fig. 12

Table 1. Elemental composition of TiSiC-Cr films

Coating	Elemental composition (at. %) (EDS)						C/(Ti+Cr)	Hydrogen content (at. %) (ERDA)
	Ti	Cr	Si	C	O	Fe		
M-90	33.6	6.4	2.6	52.2	4.3	0.9	1.31	0.5
M-110	32.2	6.3	2.5	54.4	3.5	1.1	1.41	0.6
M-130	29.6	6.1	2.5	56.6	4.4	0.8	1.59	1.1
A-90	27.5	6.7	3.5	58.7	3.2	0.4	1.72	2.0
A-110	21.8	5.5	3.0	66.6	2.8	0.3	2.43	3.9
A-130	19.2	5.5	2.7	70.3	2.1	0.2	2.85	6.2

Table 2. Carbon bond types, binding energies (BE), relative area (%) and  $sp^2/sp^3$  ratio

Coating	C-Ti BE (eV) (relative area %)	C-Cr/C-Ti* BE (eV) (relative area %)	C-C $sp^2$ BE (eV) (relative area %)	C-C $sp^3$ BE (eV) (relative area %)	$sp^2/sp^3$
M-90	281.6 (31.6)	282.7 (13.7)	284.7 (39.3)	285.6 (15.4)	2.6
A-90	282.1 (11.9)	283.4 (10.6)	284.7 (67.7)	286.0 (9.8)	6.9



Table 3. Summary of Raman spectroscopy results ( $\lambda$  – laser wavelength)

Coating	$\lambda$ (nm)	G peak ( $\text{cm}^{-1}$ )	$I_D/I_G$
M-90	488	1554	0.53
A-90		1569	0.66

Table 4. Deposition rate ( $D_R$ ), hardness (H) and adhesion (scratch test critical load ( $L_c$ ))

Coating	$D_R$ (nm/min)	H (GPa)	$L_c$ (N)
M-90	$47.2 \pm 1.7$	$26.3 \pm 0.8$	$27 \pm 2$
M-110	$51.1 \pm 1.7$	$28.7 \pm 0.9$	$25 \pm 2$
M-130	$53.8 \pm 1.8$	$29.8 \pm 0.9$	$27 \pm 2$
A-90	$67.3 \pm 1.9$	$41.3 \pm 1.1$	$26 \pm 2$
A-110	$71.9 \pm 1.9$	$42.9 \pm 1.2$	$21 \pm 2$
A-130	$77.5 \pm 2.0$	$45.1 \pm 1.2$	$23 \pm 2$

Table 5. The atomic concentrations of elements inside the wear tracks (EDS)

Coating	Elemental composition (at. %)					
	Ti	Cr	Si	C	Fe	O
M-90	25.3	3.9	2.4	34.9	8.9	24.6
M-110	22.9	3.8	2.3	30.5	7.8	32.7
M-130	15.6	2.5	2.4	33.9	13.1	32.5
A-90	27.4	6.8	3.8	53.8	0.6	7.6
A-110	21.8	5.7	3.2	64.5	0.4	4.4
A-130	20.5	5.2	2.6	69.6	0.4	2.7